2016 IEEE/RSJ International Conference on Intelligent Robots and Systems (IROS)
Daejeon Convention Center
October 9-14, 2016, Daejeon, Korea

Disturbance Compensation and Step Optimization for Push Recovery

Robert J. Griffin, Alexander Leonessa* and Alan Asbeck

***Abstract*— To operate in human environments, robots must be able to withstand external disturbances. Small disturbances can be stabilized through momentum regulation, but larger ones require steps to prevent falling. This work presents two new techniques for disturbance rejection. The first is an extension of divergent component of motion (DCM) and capture point tracking controllers that augments a PI feedback control law with a disturbance observer. This is used to estimate transient disturbances through momentum-rate-of-change error. For larger disturbances, we present a novel optimization-based framework based on the DCM dynamics that uses a quadratic program to compute the desired ground reaction forces and recovery step location. Using optimization gives a flexibility that enables planning angular-momentum-rate-of-change trajectories to help reduce recovery step length. We then illustrate the effectiveness of these methods with hardware and simulation experiments of the THOR humanoid.**

I. Introduction

To be viably used in real world environments, humanoid robots must be able to reliably reject external disturbances. Working in anything but the most rigid of settings requires the ability to navigate uncertain terrain and obstacles, inevitably leading to the robot being tripped or bumped. Compliant force control helps mitigate some of these concerns, but when met with a large enough disturbance, the robot must step to retain its balance. Therefore, for bipedal robots to realize their full potential, the design of appropriate balance and step recovery controllers is essential.

As noted in [1, 2], responses to external disturbances can be generally broken into three categories in response to appropriately larger disturbances. For smaller disturbances, shifting the center of pressure (CoP) with ankles torques is adequate. However, the CoP is limited by the unilateral and friction limited nature of the contact points. Because of this, larger disturbances may require the generation of angular momentum for stabilization. In [3], the authors demonstrated that this behavior emerges naturally when using momentum-based whole-body control strategies, by windmilling and forward lunging. The magnitude of realizable angular momentum, however, is limited, requiring one or more steps to be taken to stabilize the largest disturbances. Without stepping, the robot would simply fall when met with a large enough disturbance.

Control of linear momentum has been demonstrated as a successful approach for maintaining balance, particularly in whole-body control frameworks [3–7]. Linear momentum was controlled in [7] by including the minimization of deviation from the desired CoP trajectories in their quadratic program (QP) based whole-body controller. The CoP dynamics were also included in the whole-body control QP as the minimization of the cost-to-go of an infinite horizon LQR problem in [6]. Alternatively, the capture point (CP) [1] and 3D divergent component of motion (DCM) [8] have been used with state feedback to effectively control the CoM and linear momentum [4, 9–12]. These PI control laws, however, have an inherent limitation when it comes to transient disturbances, as the control effort relies entirely on tracking error. In this work, we propose incorporating a disturbance observer (DOB) to counter external disturbances before they result in tracking error too large to handle through PI control.

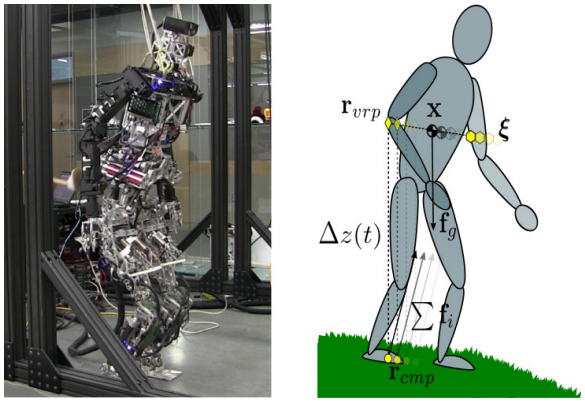

Fig. 1. Left: Push recovery using feedback on THOR. Right: DCM dynamics and external forces acting on a humanoid.

Large disturbances, however, still require adequate methods to determine the appropriate time and place to step. In [13], stabilizing zero moment point (ZMP) trajectories were generated by optimizing three step positions, while [14] optimizes just one step position to cause the ZMP to lie in the middle of the adjusted base of support. In [15], the authors determine the step locations from the rimless wheel model as an alternative to inverted pendulum methods. Perhaps the most famous, [1] introduced the CP as the point on the ground to place the ground reaction forces to bring the CoM motion to rest at any point in time, and also addresses using angular momentum for recovery to define capture regions. In this paper, we extend the concept of determining step location based on CP dynamics to the three-dimensional DCM. We also cast it in a novel, optimization-based formulation, which allows us to normalize the generation of angular momentum with respect to the robot's mass. This formulation guarantees the optimality of the generated stabilizing forces for the given initial conditions.

The authors are with the Mechanical Engineering Department at Virginia Tech. (e-mail: {robert.griffin, leonessa, aasbeck}@vt.edu)

This work is supported by NSF award No. 1525972.

*This material is based upon work supported by (while serving at) the National Science Foundation.

This paper is organized as follows: Section II reviews the DCM control and planning formulations presented in [4]. Section III introduces a new DCM disturbance-observer based momentum control law. Section IV presents the reactive step planner using a QP formulation. Finally, Section V presents experiments to validate the proposed methodologies.

II. Divergent Component of Motion Background

Due to the non-linearities and high dimensionality of humanoid robot dynamics, reduced-order models are often employed for real-time solutions. This is often analyzed using CoM models and ground reaction forces. The three-dimensional DCM introduced in [8] results from the transformation of the CoM state into stable and unstable first order components, as shown in Fig. 1.

A. DCM Defintion

The DCM can be described as the three dimensional point at which the CoM will come to rest, and is defined by [4]

$$\boldsymbol{\xi} = \mathbf{x} + \frac{1}{\omega(t)}\dot{\mathbf{x}}, \tag{1}$$

where $\mathbf{x}$ and $\dot{\mathbf{x}}$ are the CoM position and velocity and $\omega(t) = \sqrt{\frac{g}{\Delta z_{com}(t)}}$ is the natural frequency of the inverted pendulum given the CoM height Δz_{com}. The natural frequency given a fixed CoM height is referred to as ω_0. The DCM dynamics are given by differentiating the DCM definition, defined as

$$\dot{\boldsymbol{\xi}} = \left(\omega - \frac{\dot{\omega}}{\omega}\right)(\boldsymbol{\xi} - \mathbf{r}_{vrp}), \quad \dot{\boldsymbol{\xi}} = \omega_0 (\boldsymbol{\xi} - \mathbf{r}_{vrp}), \tag{2}$$

for the time-varying and invariant versions, where $\mathbf{r}_{vrp}$ represents the virtual repellent point (VRP) [8]. From these definitions, it can be seen that the DCM is repelled away from the VRP at a rate proportional to their separation. For the time-invariant case, the VRP is defined as

$$\mathbf{r}_{vrp} = \mathbf{r}_{ecmp} + [0, 0, \Delta z_{com}]^T, \tag{3}$$

where $\mathbf{r}_{ecmp}$ represents the enhanced centroidal moment pivot [8], defined as

$$\mathbf{r}_{ecmp} = \mathbf{x} - \frac{\sum \mathbf{f}_c}{m\omega_0^2} = \mathbf{r}_{cop} + \frac{1}{mg}[\tau_y, -\tau_x, 0]^T, \tag{4}$$

where $\mathbf{f}_c$ represents the external contact forces, and τ are torques about the center of mass. Note that the eCMP is equivalent to the CMP when it intersects the ground [4].

Balance can be achieved using the DCM by commanding the VRP that results in the DCM moving to a desired position. As the centroidal dynamics are asymptotically stable with respect to the DCM, this indirectly stabilizes the CoM. While commanding VRP setpoints outside the base of support is possible, the CoP is restricted to remaining inside it, requiring the generation of angular momentum, from Eqs. (3) and (4). Kinematic and dynamic limitations on the magnitude of realizable angular momentum define the region in which the DCM can be stabilized. This requires the robot to step and change the base of support to keep from falling when met with large disturbances.

B. Tracking Controller

To track the desired DCM during both stepping and standing motions, the control law defined in [4] can be used,

$$\mathbf{r}_{vrp} = \boldsymbol{\xi} - \frac{1}{\omega - \frac{\dot{\omega}}{\omega}}(\dot{\boldsymbol{\xi}}_r + \underbrace{\mathbf{k}_\xi (\boldsymbol{\xi}_r - \boldsymbol{\xi}) + \mathbf{k}_\Xi \int (\boldsymbol{\xi}_r - \boldsymbol{\xi})\, dt}_{PI(\boldsymbol{\xi})}), \tag{5}$$

where $\boldsymbol{\xi}_r$ and $\dot{\boldsymbol{\xi}}_r$ are the reference DCM position and velocity and $\mathbf{k}_\xi$ and $\mathbf{k}_\Xi$ are non-negative feedback gains. The first term, $\dot{\boldsymbol{\xi}}_r$, in Eq. (5) is designed to cancel the nominal unstable DCM dynamics in Eq. (2), while the second is a proportional-integral (PI) controller. The desired linear momentum-rate-of-change for the whole-body controller can then be found from Eq. (3) as

$$\dot{\mathbf{l}}_r = m\left(\omega^2 - \dot{\omega}\right)(\mathbf{x} - \mathbf{r}_{vrp}). \tag{6}$$

This controller has been demonstrated to work well for standing and stepping on a variety of terrain [16].

III. Momentum Disturbance Observer

Balance controllers often rely on state feedback to stabilize tracking errors [1, 3, 4, 8, 10, 12]. These controllers aim to cancel error caused by a variety of sources including poor joint torque tracking, environmental uncertainties and external disturbances. Sources of error can be generally placed in two categories: persistent disturbances, such as those resulting from poor joint tracking, and transient disturbances, such as from being pushed. While basic PI controllers can provide good tracking [16], separate control actions for persistent and transient disturbances have the potential for performance improvements. Disturbance observers (DOB) have been shown to improve steady-state tracking and disturbance rejection in force-controlled actuators [17–19]. We present below a novel adaptation of this approach to momentum-controlled robots.

The measured linear momentum-rate-of-change, $\dot{\hat{\mathbf{l}}}$, can be found by fusing filtered force-torque measurements from the feet with the momentum-rate-of-change calculated from the rigid-body dynamics. $\dot{\hat{\mathbf{l}}}$ can be broken into the resulting commanded momentum-rate-of-change from a tracking law or whole-body controller, $\dot{\mathbf{l}}_a$, and some unknown external disturbance, $\dot{\hat{\mathbf{l}}}_d$,

$$\dot{\hat{\mathbf{l}}} = \dot{\mathbf{l}}_a + \dot{\hat{\mathbf{l}}}_d. \tag{7}$$

In this case, $\dot{\hat{\mathbf{l}}}_d$ encodes not only external disturbances, but unmodeled plant dynamics. As $\dot{\hat{\mathbf{l}}}_d$ is already filtered, filtering $\dot{\hat{\mathbf{l}}}$ is not necessary. Due to the direct relation of

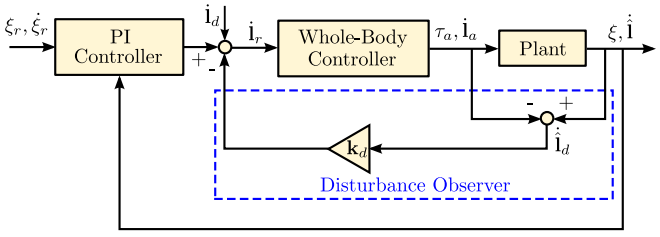

Fig. 2. DCM tracking control law augmented with momentum-rate-of-change disturbance observer.

the momentum-rate-of-change to the disturbance, no inverse plant is needed, a departure from traditional DOBs. Defining the PI controller in Eq. (5), denoted as $PI(\boldsymbol{\xi})$, in terms of momentum and introducing a term to cancel the estimated momentum disturbance results in

$$\dot{\mathbf{l}}_r = m\omega\left(\dot{\boldsymbol{\xi}}_r - \left(1 - \frac{\dot{\omega}}{\omega^2}\right)\dot{\mathbf{x}} + PI(\boldsymbol{\xi})\right) - \mathbf{k}_d\dot{\hat{\mathbf{l}}}_d, \tag{8}$$

where $\mathbf{k}_d$ is a constant gain on the DOB's control action. This control augmentation is depicted by the control block diagram in Fig. 2.

Alternatively, the DOB can be lumped into a single equation to define a new, DOB-augmented time-varying DCM tracking control law

$$\mathbf{r}_{vrp} = \boldsymbol{\xi} - \frac{1}{\omega - \frac{\dot{\omega}}{\omega}}\left(\dot{\boldsymbol{\xi}}_r + \mathbf{k}_\xi\left(\boldsymbol{\xi}_r - \boldsymbol{\xi}\right) + \mathbf{k}_\Xi\int\left(\boldsymbol{\xi}_r - \boldsymbol{\xi}\right)dt - \mathbf{k}_d\frac{1}{m\omega}\dot{\hat{\mathbf{l}}}_d\right) \tag{9}$$

IV. Reactive Step Planner

Reactively stepping when met with large disturbances can work to expand the base of support, allowing placement of the VRP to stabilize the DCM dynamics, similar to the concept of the capture point [1]. Where to step can be found using the solution of the DCM dynamics, Eq. 2,

$$\boldsymbol{\xi}(t) = e^{\omega_0 t}\left(\boldsymbol{\xi}_0 - \mathbf{r}_{vrp}(t)\right) + \mathbf{r}_{vrp}(t). \tag{10}$$

Note that this is identical to the two dimensional solution for the CP dynamics. Thus, if we step to $\boldsymbol{\xi}_f = \boldsymbol{\xi}(T)$, where T is the time at the end of the swing phase, the DCM can be stabilized by placing the VRP above the center of the foot. What remains is the determination of the VRP trajectory during single support, as this determines $\boldsymbol{\xi}_f$.

In order to be dynamically feasible, the CoP must always lie inside the stance foot while stepping. While the extremum corners of the foot can be compared to determine where to apply forces, as in [11] and illustrated in Fig. 3(a), this does not necessarily guarantee the "best" selection for all cases. Instead, we can constrain the CoP by describing the support polygon as a convex polytope and cast the problem in an optimization framework, as show in Fig. 3(b). Additionally, we can reduce the required step length by allowing the CMP to leave the polytope and generate angular momentum [1]. The use of an optimization framework allows us to define

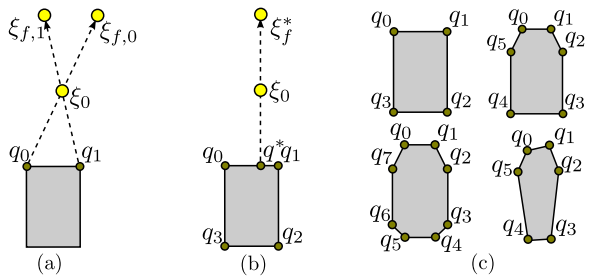

Fig. 3. (a) Dynamic selection using extremums visible from initial DCM. (b) Optimal location found using polytope definition of foot. $\boldsymbol{\xi}_f$ in (a) and (b) represent the resulting location on the DCM dynamics at heel-strike. (c) Polytope definition allows foot to be defined by any convex shape.

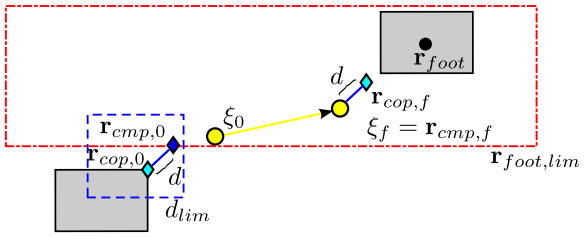

Fig. 4. Illustration of the resulting plans. DCM dynamic evolution during the swing phase is shown by the yellow arrow. The VRP is set at the DCM estimate at heel strike. Limits on the step are shown by the red box, while limits on the difference between the CMP and CoP are shown in blue.

a quadratic program (QP) that determines the CoP and CMP locations during swing by penalizing the resulting step length for recovery, while keeping angular momentum low by penalizing CMP deviation from the CoP.

A. QP Cost Function Definition

As the desired step height is determined by the environment, we only need to be concerned with finding the step position in the x-y plane. Then, if we assume constant desired CoM height, the selection of the appropriate $\mathbf{r}_{vrp}$ for stabilization is reduced to the choice of $\mathbf{r}_{cmp}$. For simplicity, we can define the $\mathbf{r}_{cop}$ and $\mathbf{r}_{cmp}$ trajectories as constant during the swing phase, $\mathbf{r}_{cop}(t) = \mathbf{r}_{cop,0}, \mathbf{r}_{cmp}(t) = \mathbf{r}_{cmp,0}, \forall t$. This is a realistic assumption, as CoP extremums are properties of the foot geometry, and, if the difference between CoP and CMP is kept low, the generated angular momentum is within the feasibility region described the kinematics of the robot. The vector of control variables for the QP is then

$$\mathbf{u} = \begin{bmatrix}\mathbf{r}_{cop,0}^T & \mathbf{r}_{cmp,0}^T & \mathbf{r}_{cmp,f}^T\end{bmatrix}^T, \tag{11}$$

where $\mathbf{r}_{cmp,f}$ is the CMP at the end of the swing phase. This results in a cost vector of size $\mathbf{u} \in \mathbb{R}^{3\times 2}$. Once we have solved for $\mathbf{r}_{cmp,0}$, we can determine $\mathbf{r}_{vrp}$ by setting the height equal to the final DCM value, $r_{vrp,z} = \xi_{f,z}$.

The cost function can then be defined as

$$\begin{aligned}\min_u\ &\left(\mathbf{r}_{cmp,f} - \mathbf{r}_{cop,0}\right)^T\mathbf{Q}\left(\mathbf{r}_{cmp,f} - \mathbf{r}_{cop,0}\right)\\ &+\left(\boldsymbol{\xi}_f - \mathbf{r}_{cmp,f}\right)^T\mathbf{C}\left(\boldsymbol{\xi}_f - \mathbf{r}_{cmp,f}\right)\\ &+\left(\mathbf{r}_{cmp,0} - \mathbf{r}_{cop,0}\right)^T\mathbf{R}\left(\mathbf{r}_{cmp,0} - \mathbf{r}_{cop,0}\right),\end{aligned} \tag{12}$$

where $\mathbf{Q}, \mathbf{R}$ and $\mathbf{C}$ are positive-definite weighting matrices for the different objectives. The first term, weighted by $\mathbf{Q}$, minimizes the distance from the stabilizing CMP and the desired initial CoP, effectively minimizing the step length. The second term, weighted by $\mathbf{C}$, minimizes the distance between the stabilizing CMP and final DCM dynamics. By not enforcing their coincidence, the step length can be constrained to be reachable. The final objective, weighted by $\mathbf{R}$, directly minimizes the generation of angular momentum.

Then the desired footstep location can be found from the final CMP as being equal in magnitude but opposite in direction from the difference between $\mathbf{r}_{cmp,0}$ and the stance foot, as illustrated in Fig. 4. This is done to give the controller appropriate authority to cancel the angular momentum generated during the step, and provides a safety margin against poor tracking.

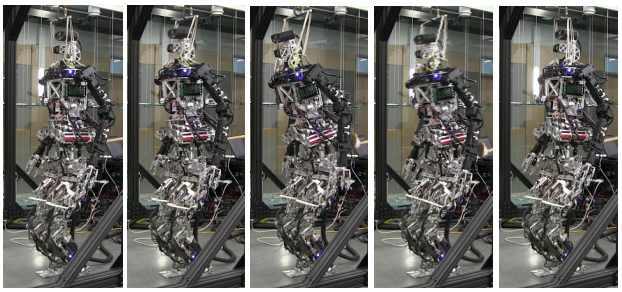

Fig. 5. Time-lapse of THOR having external disturbance applied to pelvis

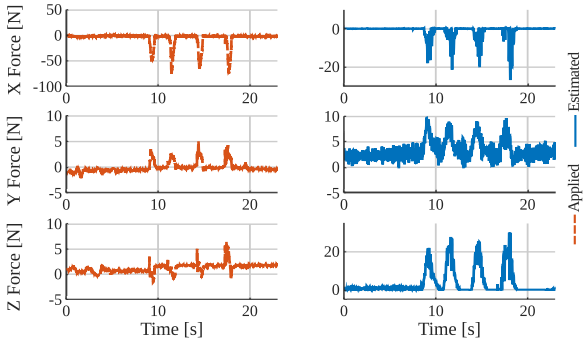

Fig. 6. Plots of applied (left) and estimated disturbances (right).

B. QP Constraints

The CoP can be constrained to lie within the foot polytope by defining it as the sum of the corners of the convex hull, defined by the equations

$$\mathbf{r}_{cop,0} = \sum_{i=0}^{N} \boldsymbol{\beta}_i q_i, \quad \mathbf{1} = \sum_{i=0}^{N} \boldsymbol{\beta}_i, \quad \boldsymbol{\beta}_i \geq 0, \forall i, \tag{13}$$

where q_i represents the i^{th} corner of the convex region with N corners, and $\boldsymbol{\beta}_i$ is a multiplier that determines the CoP's location. This allows the control vector to be rewritten as

$$\mathbf{u} = \begin{bmatrix} \boldsymbol{\beta}_i^T & \mathbf{r}_{cmp,0}^T & \mathbf{r}_{cmp,f}^T \end{bmatrix}^T, \tag{14}$$

of size $\mathbf{u} \in \mathbb{R}^{(N+2)\times 2}$. Another advantage of using this optimization constraint is it allows more complex convex descriptions of the support shape, as illustrated in Fig. 3(c).

Simple constraints on the maximum deviation of the CMP from the CoP are also implemented. Maximum and minimum forward and lateral step lengths are enforced, defining a rectangular area of reachability. These are illustrated by the blue and red boxes in Fig. 4, respectively. The formulation allows more complex constraints if desired, as long as they maintain their convexity. This can include velocity constraints on the foot to address limited actuator bandwidths and velocities, or constraints to define areas that are "safe" to step as convex planes, but are not implemented in this paper.

C. Trajectory Planning

During the swing state, the desired DCM trajectory is found in the x-y plane using Eq. (10) and the calculated CMP and CoP locations. These represent the maximum control authority of the robot. After heel strike, the desired VRP is moved to the DCM setpoint as quickly as possible, stabilizing the DCM dynamics. The desired DCM trajectory during double support is found using the reverse time integration method presented in [4]. This same method is used to find the vertical DCM trajectory during swing.

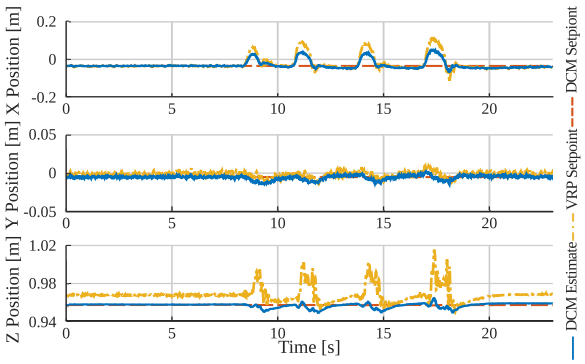

Fig. 7. Plots of DCM setpoint, estimate, and VRP setpoint while being disturbed.

V. Results

All hardware experiments were conducted on the $59kg$ Tactical Hazardous Operation Robot (THOR) compliant humanoid. Momentum setpoints were achieved using the whole-body controller described in [3].

A. DCM Disturbance Observer

Fig. 5 shows a time-lapse of THOR recovering from an external disturbance applied to the pelvis using the proposed DCM controller. A 6-axis load cell was used to collect data on the applied disturbance, presented in the top left of Fig. 6. The DOB was set up with a deadband of 3, 5, and 20 N in the x, y and z directions. A scaling factor of $\mathbf{k}_d = 0.7$ was then applied to the disturbance estimate in the z direction.

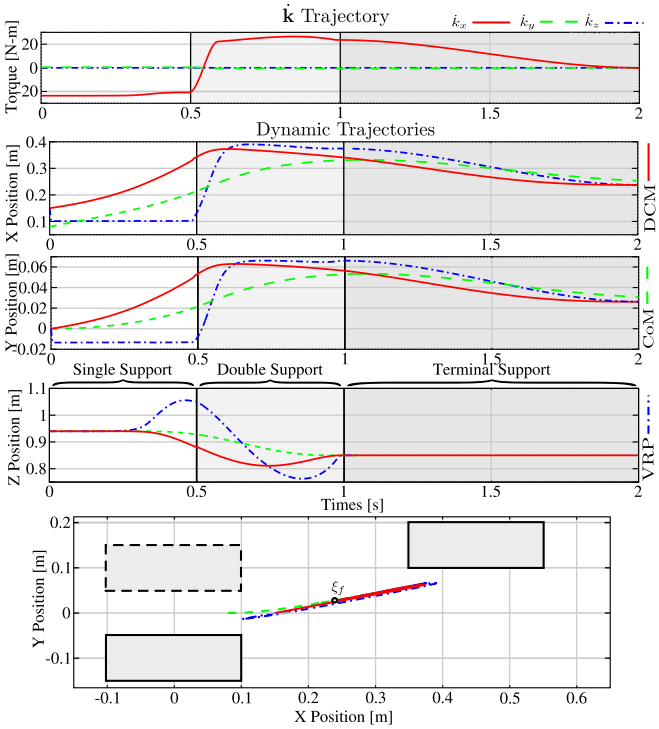

Fig. 8. Angular momentum-rate-of-change, DCM, CoM and VRP plans generated using proposed optimization based framework for recovery footstep selection.

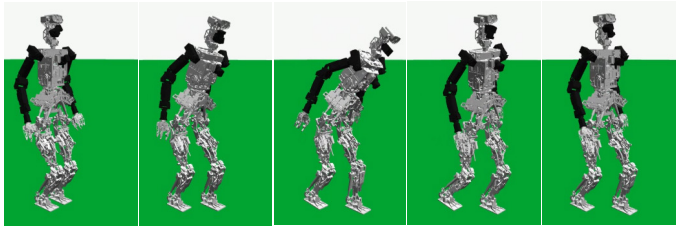

Fig. 9. Time-lapse of a simulation of a reactive step from applying a $140N$ forward disturbance for $0.25s$ to THOR's pelvis.

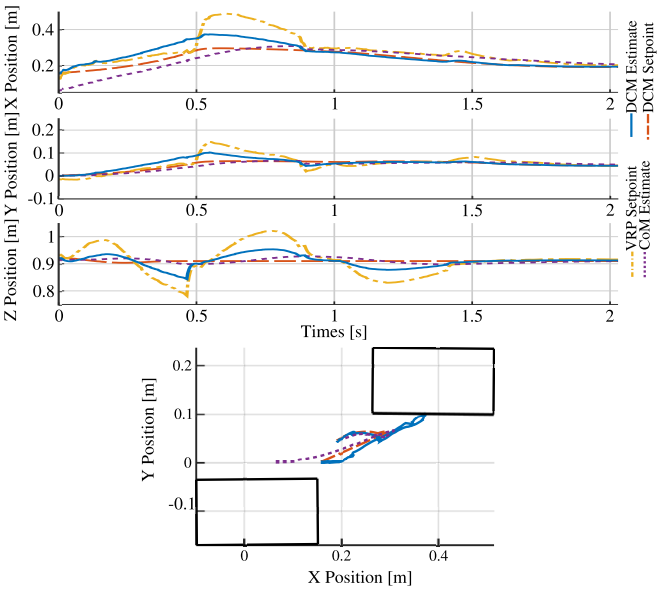

Fig. 10. Simulation data from a reactive step caused by applying a $140N$ forward disturbance for 0.25 to THOR's pelvis.

A maximum disturbance of approximately 75 N was applied in this experiment. As can be seen in the right of Fig. 6, the DOB accurately estimated the duration, timing, and direction of the applied disturbances. The magnitude estimate differed, though, due to a variety of factors, including filtering, applied deadband, and modeling errors. Additionally, the DOB estimated large vertical disturbances, possibly due to poor momentum tracking or forces being absorbed through the compliant actuators in the legs.

Using $\mathbf{k}_\xi$ and $\mathbf{k}_\Xi$ gains of 2 and 0.75 with a higher $\mathbf{k}_\xi$ gain of 7.5 in the z direction, THOR was able to quickly recover from the applied disturbances, as shown in Fig. 7. The incorporation of the DOB provided rapid changes in the commanded VRP setpoint and desired momentum-rate-of-change, allowing the DCM to be quickly stabilized. The peak disturbance estimate of approximately 25 N represents an additional shift of the VRP location of approximately 4cm. This translates to control action that does not have to be absorbed by tracking error feedback, representing faster stabilization of the robot independent of position error.

B. Reactive Stepping

1) Planning: Fig. 8 shows sample trajectories generated using the proposed optimization framework for reactive stepping. The initial conditions for this plan are $\boldsymbol{\xi}_0 = [0.15, 0, 0.94]\, m$, $0.05m$ outside the support polygon. The optimization weights are selected as $\mathbf{Q} = [0.001, 0.001]$, $\mathbf{R} = [5, 0.3]$ and $\mathbf{C} = [0.1, 0.1]$, in x and y. A rectangular polytope is used to describe the 10x20 cm foot. The single and double support stepping durations were chosen as $0.5s$ each, with an additional $1s$ of double support at the end to return the DCM to the center of the base of support. The desired footstep location to capture the DCM dynamics was found from the optimization to be $[0.475, 0.152, 0]\, m$. The average planning for both optimization of footstep location and dynamic trajectory generation time using QuadProg++ was $4.03ms$, enabling hardware implementation within our control framework running at 125 Hz. The speed can potentially be increased by decreasing the dynamic planning algorithm time or switching to faster optimization software.

2) Simulation: Fig. 9 shows time-lapse images of a reactive step using the Gazebo physics simulator. A $140N$ forward disturbance was applied to THOR's pelvis for $0.25s$, representing a fairly hard, long push. When the DCM deviated outside the support polygon by $1.5cm$, the reactive step module was activated. Larger than that results in too large a step to recover using angular momentum. Single support and double support durations of $0.5s$ were used, with a terminal support duration of $1s$ to return the DCM to the center of the support polygon. Using the same optimization weights from earlier, the desired step location is computed to be $[0.40, 0.16]\, m$. The resulting simulation data is shown in Fig. 10. During swing, the DCM estimate diverges faster than the DCM setpoint due to the whole-body control algorithm

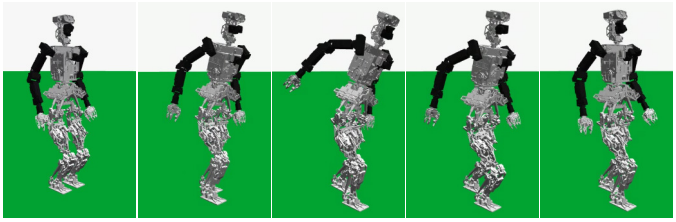

Fig. 11. Time-lapse of a simulation of a reactive step caused by applying a $120N$ forward and $110N$ lateral disturbance for 0.25 to THOR's pelvis.

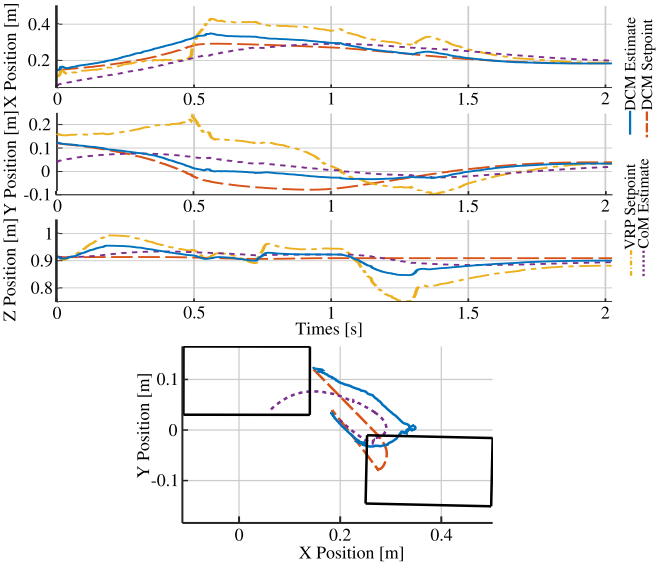

Fig. 12. Simulation data from a reactive step caused by applying a $120N$ forward and $110N$ lateral disturbance for 0.25 to THOR's pelvis.

attempting to limit the generation of angular momentum. However, once in double support, the proposed DCM controller is able to rapidly stabilize the DCM and CoM motions. As shown, the VRP rapidly shifts forward to stabilize the DCM immediately following heel strike. Most importantly, the CoM maintains smooth motions during swing and double support, representing a smooth recovery from large pushes.

A second experiment is shown in Fig. 11. This time, a $120N$ forward disturbance is applied with an additional $110N$ lateral disturbance to THOR's pelvis for the same duration as the first experiment. As can be seen in Fig. 12, when the recovery step is begun, the DCM and CoM are near the left foot. The resulting step location is to step with the right foot inward and forward to $[0.395, -0.053]\,m$, even though the robot was pushed to the left This requires the shortest step length given the current dynamic state, as stepping with the left foot would require a very wide, long step. In this scenario, the DCM estimate tracked the setpoint better than seen in Fig. 10, due to the greater initial control authority from the DCM starting near one foot, rather than in the middle of the base of support. Again, the resulting CoM motions are smooth, symbolizing a smooth recovery step.

VI. Conclusion

This work presents two new techniques to deal with external disturbances. The first is an extension of standard DCM and CP tracking controllers which augments a PI feedback control law with a disturbance observer (DOB). This is used to estimate transient disturbances through momentum-rate-of-change error. The second is a novel optimization framework based on the unstable DCM dynamics that uses a quadratic program to compute the desired ground reaction forces and recovery step location. The flexibility given by the optimization formulation enables planning angular momentum-rate-of-change trajectories to help with push recovery. The performance of the new controller was evaluated through hardware experiments with the compliant THOR humanoid. Reactive stepping was tested using simulations of THOR, subject to forward pushes and simultaneous forward and lateral pushes. Hardware testing of the stepping module was not possible due to limited actuator speeds, but should be realizable on robot platforms with faster actuation.

The benefits of the DOB-based controller is currently being tested while walking as well. By focusing on transient inputs, the DOB may help eliminate tracking errors produced by impacts during heel-strike. Additionally, the reactive stepping algorithm is currently being expanded into a full model-predictive controller, as including the entire dynamic trajectories may improve the angular momentum trajectories, enforcing limits on the total angular momentum at the planning phase. More complex but descriptive constraints on reachability areas to allow step over are being investigated. Inclusion of angular momentum when planning DCM trajectories for walking is also being explored.

References

[1] J. Pratt, J. Carff, S. Drakunov, and A. Goswami, "Capture Point: A Step toward Humanoid Push Recovery," in *Humanoid Robots (Humanoids), 6th IEEE-RAS International Conference on*, Dec 2006, pp. 200–207.

[2] B. Stephens, "Humanoid push recovery," in *Humanoid Robots (Humanoids), 7th IEEE-RAS International Conference on*, Nov 2007, pp. 589–595.

[3] M. A. Hopkins, D. W. Hong, and A. Leonessa, "Compliant locomotion using whole-body control and Divergent Component of Motion tracking," in *Robotics and Automation (ICRA), IEEE International Conference on*, May 2015.

[4] M. A. Hopkins, D. W. Hong, and A. Leonessa, "Humanoid locomotion on uneven terrain using the time-varying Divergent Component of Motion," in *Humanoid Robots (Humanoids), 14th IEEE-RAS International Conference on*, Nov 2014.

[5] T. Koolen, T. De Boer, J. Rebula, A. Goswami, and J. Pratt, "Capturability-based analysis and control of legged locomotion, part 1: Theory and application to three simple gait models," *The International Journal of Robotics Research*, vol. 31, no. 9, pp. 1094–1113, Aug 2012.

[6] S. Kuindersma, R. Deits, M. Fallon, A. Valenzuela, H. Dai, F. Permenter, T. Koolen, P. Marion, and R. Tedrake, "Optimization-based locomotion planning, estimation, and control design for Atlas," *Autonomous Robots*, vol. 40, no. 3, pp. 429–455, 2016.

[7] S. Feng, E. Whitman, X. Xinjilefu, and C. G. Atkeson, "Optimization based full body control for the Atlas robot," in *Humanoid Robots (Humanoids), 14th IEEE-RAS International Conference on*, Nov 2014.

[8] J. Englsberger, C. Ott, and A. Albu-Schaffer, "Three-dimensional bipedal walking control using Divergent Component of Motion," in *Intelligent Robots and Systems (IROS), IEEE/RSJ International Conference on*, Nov 2013, pp. 2600–2607.

[9] J. Englsberger and C. Ott, "Integration of vertical COM motion and angular momentum in an extended Capture Point tracking controller for bipedal walking," in *Humanoid Robots (Humanoids), 12th IEEE-RAS International Conference on*, Nov 2012, pp. 183–189.

[10] T. Koolen, J. Smith, G. Thomas, S. Bertrand, J. Carff, N. Mertins, D. Stephen, P. Abeles, J. Englsberger, S. McCrory, J. van Egmond, M. Griffioen, M. Floyd, S. Kobus, N. Manor, S. Alsheikh, D. Duran, L. Bunch, E. Morphis, L. Colasanto, K.-L. Ho Hoang, B. Layton, P. Neuhaus, M. Johnson, and J. Pratt, "Summary of team IHMC's Virtual Robotics Challenge entry," in *Humanoid Robots (Humanoids), 13th IEEE-RAS International Conference on*, Oct 2013.

[11] J. Pratt, T. Koolen, T. De Boer, J. Rebula, S. Cotton, J. Carff, M. Johnson, and P. Neuhaus, "Capturability-based analysis and control of legged locomotion, part 2: Application to M2V2, a lower body humanoid," *The International Journal of Robotics Research*, vol. 31, no. 10, pp. 1117–1133, 2012.

[12] M. Morisawa, S. Kajita, F. Kanehiro, K. Kaneko, K. Miura, and K. Yokoi, "Balance control based on Capture Point error compensation for biped walking on uneven terrain," in *Humanoid Robots (Humanoids), 12th IEEE-RAS International Conference on*, Nov 2012, pp. 734–740.

[13] J. Urata, K. Nshiwaki, Y. Nakanishi, K. Okada, S. Kagami, and M. Inaba, "Online decision of foot placement using singular LQ preview regulation," in *Humanoid Robots (Humanoids), 2011 11th IEEE-RAS International Conference on*, Oct 2011, pp. 13–18.

[14] B. Stephens and C. Atkeson, "Dynamic balance force control for compliant humanoid robots," in *Intelligent Robots and Systems (IROS), IEEE/RSJ International Conference on*, Oct 2010, pp. 1248–1255.

[15] S. kook Yun and A. Goswami, "Momentum-based reactive stepping controller on level and non-level ground for humanoid robot push recovery," in *Intelligent Robots and Systems (IROS), 2011 IEEE/RSJ International Conference on*, Sept 2011, pp. 3943–3950.

[16] M. A. Hopkins, R. J. Griffin, A. Leonessa, B. Y. Lattimer, and T. Furukawa, "Design of a compliant bipedal walking controller for the DARPA Robotics Challenge," in *Humanoid Robots (Humanoids), 2015 15th IEEE-RAS International Conference on*, 2015.

[17] K. Kong, J. Bae, and M. Tomizuka, "Control of rotary series elastic actuator for ideal force-mode actuation in human-robot interaction applications," vol. 14, no. 1, pp. 105–118, 2009.

[18] N. Paine, S. Oh, and L. Sentis, "Design and control considerations for high-performance series elastic actuators," *Mechatronics, IEEE/ASME Transactions on*, vol. 19, no. 3, pp. 1080–1091, June 2014.

[19] M. Hopkins, S. Ressler, D. Lahr, A. Leonessa, and D. Hong, "Embedded joint-space control of a series elastic humanoid," in *Intelligent Robots and Systems (IROS), 2015 IEEE/RSJ International Conference on*, Sept 2015, pp. 3358–3365.